AMERICAN SOCIETY FOR MICROBIOLOGY | Journal of Bacteriology®

RESEARCH ARTICLE

Contributions of the N- and C-Terminal Domains of Initiation Factor 3 to Its Functions in the Fidelity of Initiation and Antiassociation of the Ribosomal Subunits

Shreya Ahana Ayyub,[a] Divya Dobriyal,[a] Umesh Varshney[a,b]

Department of Microbiology and Cell Biology, Indian Institute of Science, Bangalore, India[a]; Jawaharlal Nehru Centre for Advanced Scientific Research, Jakkur, Bangalore, India[b]

ABSTRACT Initiation factor 3 (IF3) is one of the three conserved prokaryotic translation initiation factors essential for protein synthesis and cellular survival. Bacterial IF3 is composed of a conserved architecture of globular N- and C-terminal domains (NTD and CTD) joined by a linker region. IF3 is a ribosome antiassociation factor which also modulates selection of start codon and initiator tRNA. All the functions of IF3 have been attributed to its CTD by *in vitro* studies. However, the *in vivo* relevance of these findings has not been investigated. By generating complete and partial IF3 (*infC*) knockouts in *Escherichia coli* and by complementation analyses using various deletion constructs, we show that while the CTD is essential for *E. coli* survival, the NTD is not. Polysome profiles reaffirm that CTD alone can bind to the 30S ribosomal subunit and carry out the ribosome antiassociation function. Importantly, in the absence of the NTD, bacterial growth is compromised, indicating a role for the NTD in the fitness of cellular growth. Using reporter assays for *in vivo* initiation, we show that the NTD plays a crucial role in the fidelity function of IF3 by avoiding (i) initiation from non-AUG codons and (ii) initiation by initiator tRNAs lacking the three highly conserved consecutive GC pairs (in the anticodon stem) known to function in concert with IF3.

IMPORTANCE Initiation factor 3 regulates the fidelity of eubacterial translation initiation by ensuring the formation of an initiation complex with an mRNA bearing a canonical start codon and with an initiator tRNA at the ribosomal P site. Additionally, IF3 prevents premature association of the 50S ribosomal subunit with the 30S preinitiation complex. The significance of our work in *Escherichia coli* is in demonstrating that while the C-terminal domain alone sustains *E. coli* for its growth, the N-terminal domain adds to the fidelity of initiation of protein synthesis and to the fitness of the bacterial growth.

KEYWORDS initiation with AUA, initiation with AUU, 3GC base pairs, initiator tRNA

Received 21 January 2017 **Accepted** 14 March 2017

Accepted manuscript posted online 20 March 2017

Citation Ayyub SA, Dobriyal D, Varshney U. 2017. Contributions of the N- and C-terminal domains of initiation factor 3 to its functions in the fidelity of initiation and antiassociation of the ribosomal subunits. J Bacteriol 199:e00051-17. https://doi.org/10.1128/JB.00051-17.

Editor Richard L. Gourse, University of Wisconsin—Madison

Address correspondence to Umesh Varshney, varshney@mcbl.iisc.ernet.in.

The process of translation initiation is the most highly regulated step of protein synthesis, where the three initiation factors serve to establish this tight scrutiny. Initiation factor 3 (IF3) is one such factor which acts as an antiassociation factor for the two ribosomal subunits (1). IF3 from *Escherichia coli* is composed of 180 amino acids (aa) and is encoded by the essential *infC* gene (2). Structurally, IF3 can be divided into globular N- and C-terminal domains (NTD and CTD) joined by a linker region. The most important functions of IF3 include ribosome antiassociation (1, 3), shifting 30S-bound mRNA from standby to the P site (4), and its fidelity functions (5, 6). The fidelity function of IF3 entails ejection of incorrect (elongator) tRNAs to allow preferential selection of

the initiator tRNA, $tRNA^{fMet}$ (referred to as "i-tRNA" here). According to the *in vitro* data, most of the functions of the full-length molecule can be attributed to the CTD (7), while the NTD merely modulates the thermodynamic stability of the 30S-IF3 complex. However, according to structural studies, while the NTD is modeled to contact the elbow region of fMet-$tRNA^{fMet}$ (8), the CTD is engaged in interactions with h23, h24, and h45 of the 16S rRNA (9). More recently, studies reported from the Ramakrishnan laboratory have also noted the presence of the CTD near h45 and h24. And, while the linker showed no contact with the 30S subunit, the NTD showed interactions with the elbow of i-tRNA (10). Interestingly, the fidelity function studies performed with IF3 mutants revealed that although mutations in both the NTD and CTD contribute to the loss of fidelity (11), only the CTD mutants are concomitantly defective in ribosome binding (12, 13) (see Table S1 and Fig. S1 in the supplemental material). The NTD mutants do not experience any loss of affinity to the ribosome despite a drastic loss of the fidelity function (11, 13). Therefore, it appears that the NTD directly affects the fidelity of IF3. A specific investigation of the contribution of the individual domains of IF3 to fidelity functions *in vivo* is still lacking.

Recent studies have shown that deletion of H69 (ΔH69) of 23S rRNA permits uncompromised start codon selection and rapid 50S association without simultaneous IF3 release (14). Therefore, the fidelity function of IF3 is not fully dependent on its antiassociation function. However, deletion of H69 compromises the ability of IF3 to regulate 50S association in response to different start codons, indicating that IF3 permits subunit association only once a cognate codon-anticodon pair is detected. Additionally, those studies showed that dissociation of IF3 from the ribosome is dependent on the identity of the start codon. Interestingly, work done in our laboratory has also suggested that dissociation of IF3 from the ribosome is dependent on the presence of intact 3GC base pairs in the anticodon stem (15). Therefore, the fidelity function of IF3, 50S subunit docking, and IF3 release are linked but the order of these events remains to be elucidated.

Another unexplored facet of IF3 study is the essentiality of the individual domains of IF3. Although, according to an earlier study (7), the CTD of IF3 is supposed to possess all the functions of the molecule, no study has been able to show if the CTD of IF3 can sustain a bacterial cell. In fact, overexpression of the individual CTD of IF3 has been suggested to be toxic (11). In our study, we showed that, in accordance with expectations from *in vitro* data, the CTD (also containing the linker) can indeed sustain an *E. coli infC* deletion strain. The loss of fidelity of an *infC* partial deletion strain could be ameliorated more efficiently by overexpression of the NTD than by overexpression of the CTD. Overexpression of the CTD leads to as much ribosome antiassociation activity as overexpression of the whole molecule. Thus, the two domains of IF3 have important functions; while the CTD is essential for survival of the cell, the NTD plays a vital role in the fitness of bacteria.

RESULTS

Generation and characterization of the *infC* partial deletion strain. In order to explore the *in vivo* roles of the individual domains of IF3 and their truncated derivatives (Table 1 and Fig. 1), we generated a complete *infC* deletion in the background of a native plasmid-borne IF3 (Fig. 1A, panel ii; Fig. 2A, lane 1 [2-kb band]). The deletion was carried out by introducing into *E. coli* KL16 (also referred to here as *E. coli*) a fragment of linear DNA encoding the kanamycin resistance (Kan^r) gene flanked by regions homologous to nucleotide sequences bordering the chromosomal *infC* gene. Recombination efficiency was increased by expressing λ Red recombinase proteins from the pKD46 plasmid harbored by the host (18). A complete *infC* knockout could not be generated without support, once again confirming the essentiality of IF3. However, despite previously published contrasting reports (11), we were able to generate a complete *infC* knockout when just the CTD (105 aa) of *E. coli* IF3 (EcoIF3) (IF3 here) was expressed from a plasmid (Fig. 2A, lane 2 [2-kb band]). The strain was also verified by immunoblotting and SDS-PAGE, where only the CTD could be detected (Fig. 3A, lane 4;

TABLE 1 Description of *E. coli* strains and plasmids used in this study

Strain or plasmid	Genotype or details	Reference or source
Strains		
KL16	*E. coli* K-12 *thi1 relA1 spoT1*	16
KL16 *infC*Δ55	KL16 derivative with *infC* partial deletion and insertion of a Kan^r gene in lieu of the first 55 amino acids of IF3	This study
KL16 *infC*Δ75	KL16 derivative with *infC* partial deletion and insertion of a Kan^r gene in lieu of the first 75 amino acids of IF3	This study
KL16 *infC*Δ89	KL16 derivative with *infC* partial deletion and insertion of a Kan^r gene in lieu of the first 89 amino acids of IF3	This study
KL16 Δ*infC fs*	KL16 derivative with *infC* partial deletion and insertion of a Kan^r gene in lieu of the first 55 amino acids of IF3 with an out-of-frame ATG from pKD4; this strain does not express the 125-aa truncated derivative of IF3	This study
KL16 Δ*infC*/pIF3	KL16 derivative with total *infC* deletion by insertion of a Kan^r gene, supported by pACDHEcoIF3	This study
Plasmids		
pTrcEcoIF3	*E. coli* IF3 was cloned into NdeI and HindIII sites of pTrc99C	Laboratory stock
pACDH (Tet^r)	A low-copy-number vector with pACYC ori, compatible with ColE1 origin of replication and harboring Tet^r	17
pACDHEcoIF3 (pIF3)	EcoIF3 from pTrc99c was subcloned into Ecl136II and HindIII sites of pACDH	This study
pACDHEcoIF3CTD (pCTD)	EcoIF3CTD was cloned into NcoI and HindIII sites of pACDH	This study
pACDHEcoIF3NTD (pNTD)	EcoIF3NTD was cloned into NcoI and HindIII sites of pACDH	This study
pACDHEcoIF3NTD90 (pNTD90)	EcoIF3NTD90 (90 aa) was cloned into NcoI and HindIII sites of pACDH	This study
pACDHEcoIF3NTD75 (pNTD75)	EcoIF3NTD75 (75 aa) was cloned into NcoI and HindIII sites of pACDH	This study
pKD4	Amp^r Kan^r *kan* marker is flanked by FRT sequences	18
pKD46	Amp^r; harbors λ Red recombination genes (γ, β, and *exo*)	18
$pCAT_{AUG}$	Renamed from $pRSVCAT_{2.5}$	19
$pCAT_{GUG}$	AUG initiation codon of $pCAT_{AUG}$ mutated to GUG	20
$pCAT_{UUG}$	AUG initiation codon of $pCAT_{AUG}$ mutated to UUG	20
$pCAT_{AUU}$	AUG initiation codon of $pCAT_{AUG}$ mutated to AUU	20
$pCAT_{AUA}$	AUG initiation codon of $pCAT_{AUG}$ mutated to AUA	20
$pCAT_{ACG}$	AUG initiation codon of $pCAT_{AUG}$ mutated to ACG	20
$pCAT_{am1}metY_{CUA}$	$pCAT_{am1}$ harboring mutant *metY* with CUA anticodon	21
$pCAT_{am1}metY_{CUA/3GC}$	$pCAT_{am1}metY_{CUA}$ harboring additional mutation of 3GC pairs in $metY_{CUA}$	22
$pCAT_{am1}metY_{CUA/AU-GU}$	$pCAT_{am1}metY_{CUA}$ harboring additional mutations of U39, A29, and U41 in $metY_{CUA}$	23

see also Fig. S3 in the supplemental material). We could not study shorter derivatives of the CTD (91 aa, 85 aa, and 81 aa) that lacked the linker region. Their expression, possibly due to their degradation in a strain like the *E. coli* KL16 wild type for its proteases, could not be detected. Subsequently, to investigate the functions of the NTD, we generated two versions (100 aa and 90 aa) with the linker and a shorter version

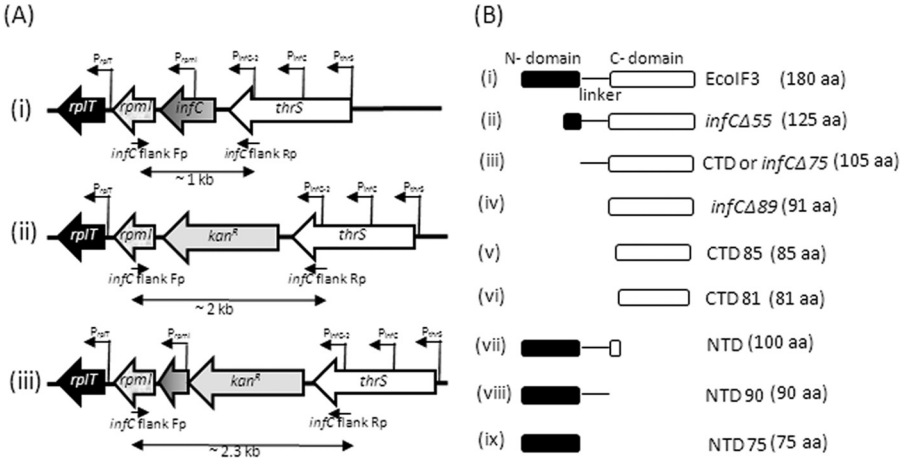

FIG 1 (A) Organization of the *thrS-infC-rpmI-rplT* locus in (i) wild-type *E. coli*, (ii) *E. coli* Δ*infC*::Kan^r, and (iii) *E. coli infC*Δ55::Kan^r. (B) Domain structure of EcoIF3 and its deletion derivatives.

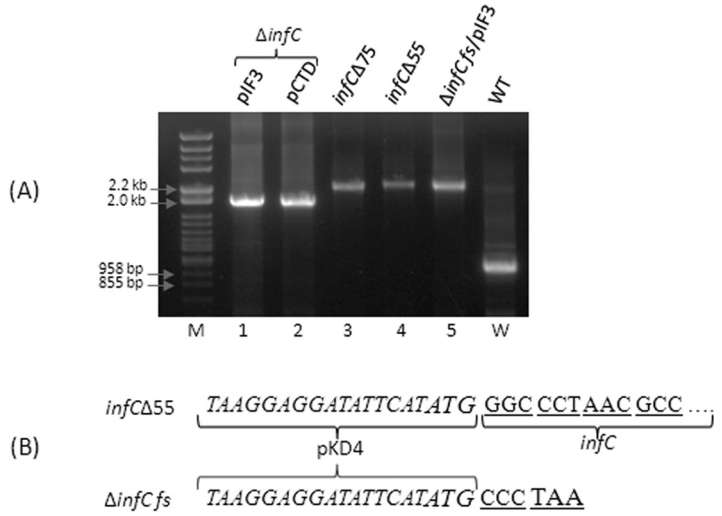

FIG 2 Verification of complete and partial *infC* knockouts. (A) Verification of indicated strains by colony PCR with *infC* flank primers. Wild type (WT [lane W]) strain, 1 kb; Δ*infC* mutant, 2 kb; *infC*Δ55 mutant, 2.3 kb. Lane M, lambda DNA digested with HincII and HindIII. (B) Depiction of initiation codon (italicized) and stop codon (underlined) in *infC*Δ55 and Δ*infC fs* strains.

(75 aa) without the linker (Fig. 1B, panels vii, viii, and ix). The derivative (called NTD here) which was 100 aa long was the only one which we could express in *E. coli* KL16 (Fig. 3B, lane 1; Fig. S2, lanes 5 to 8), and it was unable to support a full-length *infC* knockout.

In order to investigate how much of the chromosomal *infC* gene could be deleted within the limits of viability, we generated a *infC*Δ75 strain where the entire NTD had been deleted from the genome. The *infC*Δ75 strain was viable without or with IF3 support (Fig. 1B, panel iii; Fig. 2A, lane 3 [2.3-kb band]). Strain *infC*Δ89 (where the linker is not encoded along with the CTD in the genome) was not viable without complementation by IF3, probably because the encoded CTD (91 aa) was not stable (no bands corresponding to *infC*Δ89 are visible in lanes 3 and 4 in Fig. S2). Taking the data

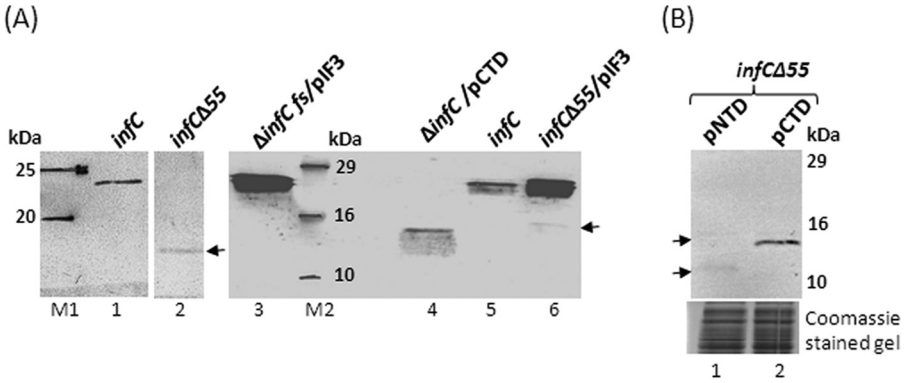

FIG 3 Western analysis performed with anti-EcoIF3 antibodies against 40 μg of cell extracts of various strains. Strains *infC*, *infC*Δ55, and Δ*infC* are *E. coli* KL16 strains that are wild type for chromosomal *infC*, deleted for the first 55 codons of chromosomal *infC* (*E. coli* KL16 *infC*Δ55) and deleted for the full length of *infC* (*E. coli* KL16 Δ*infC*), respectively. The Δ*infC fs* strain is a derivative of strain *infC*Δ55 wherein chromosomally coded IF3Δ55 cannot be produced because of a frameshift mutation (Table 1). (A) Immunoblot performed with cell extracts from the strains indicated above the lanes. The presence of plasmids, if any, in the strains is also indicated. The arrows at lanes 2 and 6 indicate the 125-aa IF3 band. Lane M1, prestained size markers (drawn over by pen). Lane M2, prestained size markers (drawn over by pen). (B) The upper panel presents an immunoblot, whereas the lower panel presents results of Coomassie-stained SDS-PAGE indicating equal loading of the cell extracts. The upper arrow indicates the 125-aa IF3 band, and the lower arrow indicates the IF3 NTD.

together, we conclude that while the CTD is essential for the survival of *E. coli*, the functions of the NTD are dispensable.

Generation of the *infC*Δ55 partial deletion strain. The promoter (P_{rpmI}) of the downstream genes *rpmI* (encoding bL35) and *rplT* (encoding bL20) is located 165 nucleotides into *infC* (Fig. 1A, panel i). P_{rpmI} is not a major promoter (24), and in the *infC*Δ75 strain, P_{rpmI} could be deleted. Nonetheless, since the change in transcription of bL35 and bL20 may have had unforeseeable effects on our studies, we decided to generate a strain where P_{rpmI} would be left unperturbed (Fig. 1A, panel iii). Accordingly, in the *infC*Δ55 strain, only the first 55 aa of the NTD were replaced with the Kan^r cassette (Fig. 2A, lane 4 [2.3-kb band]). An in-frame ATG from the Kan^r cassette was able to initiate translation of truncated IF3 (Fig. 2B), which we verified by generating a strain (Δ*infC fs* [frameshift mutation]) where the ATG was not in frame, and the resulting strain was viable only with plasmid-borne IF3 support (Fig. 2A, lane 5 [2.3 kb]). The N-terminally truncated derivative of IF3 (125 aa) was detected in the *infC*Δ55 strain (Fig. 3A, lane 2). This truncated IF3 was not detectable in the Δ*infC fs* background (Fig. 3A, compare lane 3 to lane 6). Strain *infC*Δ55 was used to study the functions of the IF3 domains.

Although the *infC*Δ55 strain was viable, compared with the wild-type parent, it was significantly compromised in its growth, as shown by an extended lag phase (Fig. S4A and B, compare curves 1 and 2) and a longer doubling time (Fig. S4C). This was either due to very low levels of the N-terminally truncated 125-aa-long IF3 in the cell or due to the absence of the NTD which might play a role in the fitness of the strain. Therefore, we expressed the full-length IF3 CTD or NTD individually in the strain. As expected, expression of IF3 restored growth of the strain to a wild-type level (Fig. S4A and B [compare curves 2 and 3 with curve 1 and the doubling times] and S4C). In contrast to previous reports (11), expression of the CTD even upon IPTG induction was not toxic (Fig. S4B, compare curves 2 and 5). However, neither overexpression of the NTD nor overexpression of the CTD significantly altered the growth of strain *infC*Δ55.

Start codon selection activity of the domains of IF3. Analysis of the fidelity of IF3 involves the scrutiny of the 3GC base pairs in the anticodon stem of i-tRNA in conjunction with the initiation codon on the mRNA (25) and the subsequent ejection of non i-tRNAs. As some earlier reports suggested a role for some residues of the NTD in the maintenance of fidelity (11) whereas others contended that all functions of IF3 were performed by its CTD (7), we decided to address this issue with a reporter-based fidelity assay. We introduced *cat* reporter gene plasmids ($pCAT_{AUG}$, $pCAT_{GUG}$, $pCAT_{UUG}$, $pCAT_{AUU}$, $pCAT_{ACG}$, and $pCAT_{AUA}$) where the AUG initiation codon was mutated to the GUG, UUG, AUU, ACG, or AUA codon (20) into the various strains to measure initiation with the cellular i-tRNA. The initiation activities were measured by chloramphenicol acetyltransferase (CAT) enzyme assays (26).

As the 3′ nucleotide of the initiation codon is inspected by IF3 (25), AUU and AUA are very poor start codons in *E. coli*. Expectedly, they showed very low levels of initiation in either the wild-type or the IF3 overexpression strains (Fig. 4A and B, bars 1 and 2). The *infC*Δ55 strain showed an 80-fold increase in initiation with the AUA codon (Fig. 4A, compare bars 1 and 3) and a 2-fold increase in initiation with the AUU codon (Fig. 4B, compare bars 1 and 3). Notably, expression of the NTD rescued the fidelity of the *infC*Δ55 strain to almost wild-type levels, in the case of AUA initiation (Fig. 4A, compare bars 3 and 4). This observation is especially remarkable considering that the NTD levels in the cell were visibly much lower than the CTD levels (Fig. 3B, compare lanes 1 and 2). Interestingly, although the results were statistically significant, expression of the CTD resulted in only a very small decrease in CAT activity compared to the strain background (strain *infC*Δ55) (Fig. 4A, compare bars 3 and 5). The increase in AUU initiation in the *infC*Δ55 strain was only 2-fold higher than the increase in the wild type (Fig. 4B, compare bars 1 and 3); therefore, there was a smaller window during which to observe the effects of CTD or NTD expression in the *infC*Δ55 strain. However, it is clear that CTD expression did not decrease initiation with the AUU start codon (Fig. 4B, compare bars

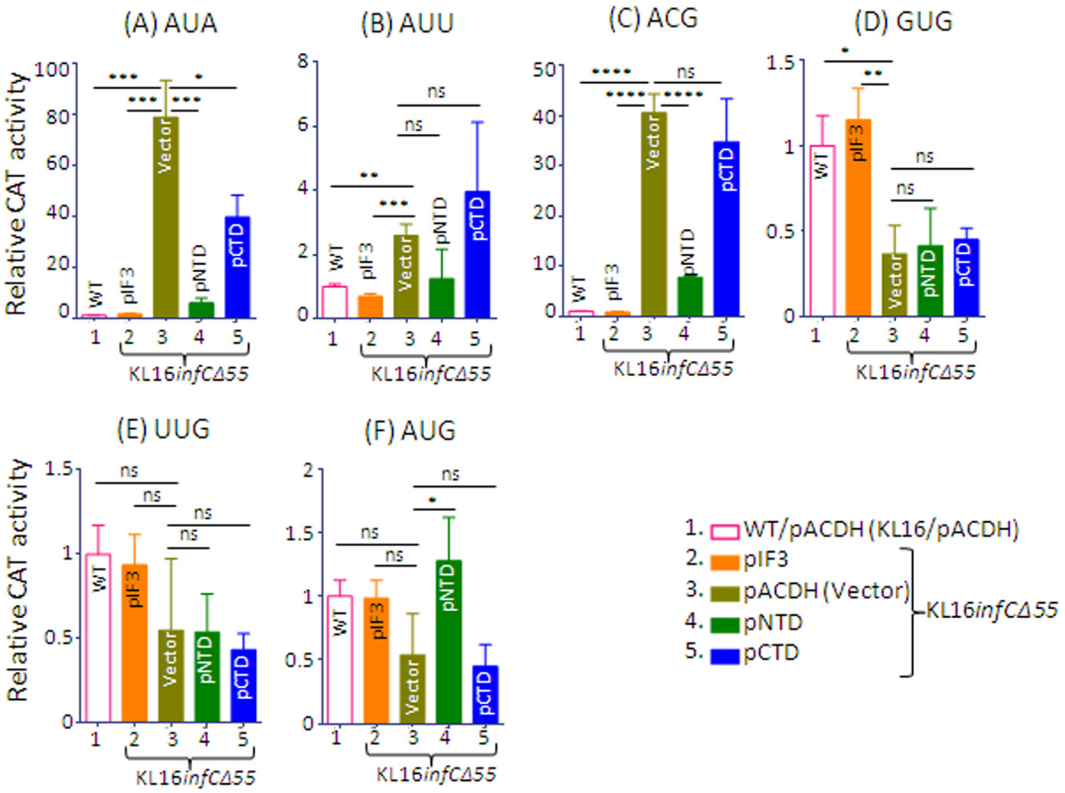

FIG 4 Initiation with various codons in the wild-type and *infC*Δ55 strains. CAT activities of strains harboring $pCAT_{AUA}$, $pCAT_{AUU}$, $pCAT_{ACG}$, $pCAT_{GUG}$, $pCAT_{UUG}$, or $pCAT_{AUG}$ were calculated relative to that of the same strain harboring $pCAT_{AUG}$. Subsequently, to allow scaling of initiation by each of the codons to units in the wild-type strain (KL16/pACDH), the relative initiation activity values determined for AUA, AUU, ACG, GUG, UUG, and AUG for the *infC*Δ55 and KL16/pACDH strains were divided by the respective relative initiation activity values determined for the KL16/pACDH strains. For reference, the average CAT activity values determined for the KL16/pACDH strains for the AUA, AUU, ACG, GUG, UUG, and AUG constructs were 0.44 ± 0.02, 0.51 ± 0.04, 0.26 ± 0.02, 16.35 ± 2.87, 21.29 ± 3.68, and 26.27 ± 3.26 pmol Cm converted/ng of total cell extract.

3 and 5). In order to investigate initiation with a second-position initiation codon mutant as a control, we used the $pCAT_{ACG}$ construct. We saw the same pattern as that seen with the AUA start codon, where the NTD decreased the elevated ACG codon initiation of the *infC*Δ55 mutant, while expression of the CTD had no effect (Fig. 4C, compare bars 3, 4, and 5). Initiation from the nearly cognate start codons GUG and UUG was lower in the *infC*Δ55 strain than in the wild type (Fig. 4D and E, compare bars 1 and 3), and the levels remained unchanged upon expression of CTD or NTD (Fig. 4C and D, compare bar 3 with bars 4 and 5). This observation further supports the concept that the rescue of fidelity by NTD (Fig. 4A and C) is a genuine phenomenon and does not simply represent an arbitrary decrease in initiation efficiency.

Anticodon stem discrimination of i-tRNA by the domains of IF3. To investigate which domains of IF3 may be capable of distinguishing i-tRNA via its extremely conserved feature of the 3GC base pairs in the anticodon stem, we generated a CAU-to-CUA anticodon change in the i-tRNA gene (*metY*) possessing a wild-type complement of the 3GC sequence ($i\text{-}tRNA_{CUA}$ or $metY_{CUA}$) or lacking the complement ($metY_{CUA/AU\text{-}GU}$, $metY_{CUA/3GC}$) to initiate translation from the *cat* reporter with a UAG start codon (21, 22). The reporter plasmids ($pCAT_{am1}metY_{CUA}$, $pCAT_{am1}metY_{CUA/AU\text{-}GU}$, and $pCAT_{am1}metY_{CUA/3GC}$) were introduced into the requisite *E. coli* strains.

In the *infC*Δ55 strain, there was a 4-fold increase in initiation with the AU-GU mutant i-tRNA (Fig. 5B, compare bars 1 and 3) and a 3-fold increase in initiation with the 3GC mutant i-tRNA (Fig. 5C, compare bars 1 and 3), indicating loss of fidelity. Once again, expression of the NTD appeared to diminish initiation with the AU-GU and 3GC mutant i-tRNAs to levels nearing those seen with initiation by them in the wild-type strain

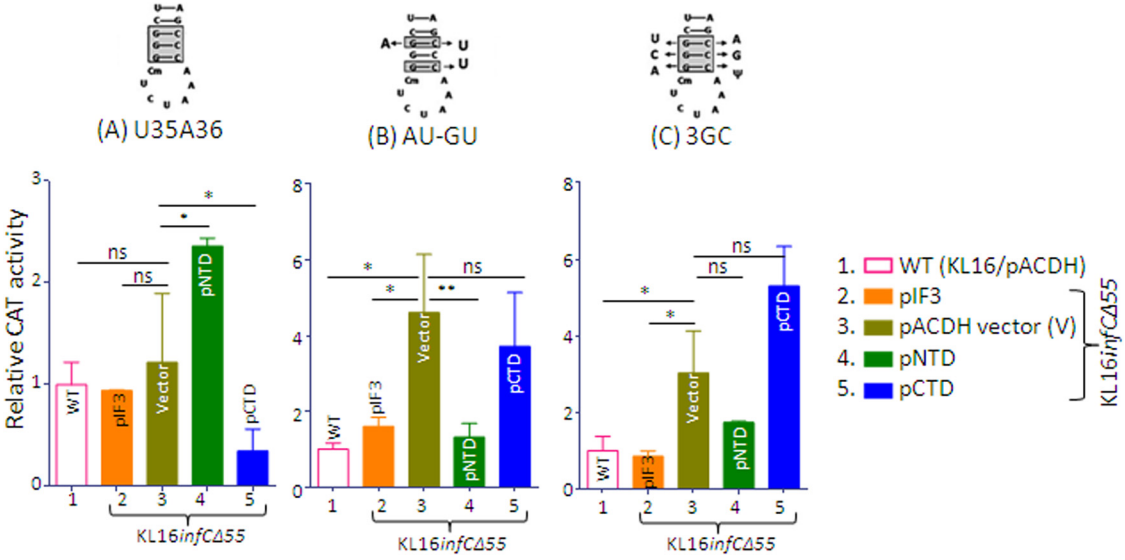

FIG 5 Initiation with 3GC base pair anticodon stem mutants of $metY_{CUA}$ in wild-type and *infC*Δ55 strains. CAT activities of strains harboring $pCAT_{am1}metY_{CUA}$, $pCAT_{am1}metY_{CUA/AU-GU}$, or $pCAT_{am1}metY_{CUA/3GC}$ were calculated relative to that of the same strain harboring $pCAT_{am1}metY_{CUA}$. Subsequently, to allow scaling of initiation by each of the i-tRNAs to units in the wild-type strain (KL16/pACDH), the relative initiation activity values determined for $pCAT_{am1}metY_{CUA/AU-GU}$ and $pCAT_{am1}metY_{CUA/3GC}$ for the *infC*Δ55 and KL16/pACDH strains were divided by the respective relative initiation activity values determined for the KL16/pACDH strain. For reference, the average CAT activity values determined for strain KL16/pACDH for the constructs $pCAT_{am1}metY_{CUA}$, $pCAT_{am1}metY_{CUA/AU-GU}$, and $pCAT_{am1}metY_{CUA/3GC}$ were 24.19 ± 5.32, 0.09 ± 0.01, and 0.16 ± 0.06 pmol Cm converted/ng of total cell extract.

(Fig. 5B and C, compare bars 3 and 4), although the rescue was not significant for the 3GC mutant i-tRNA (the difference in initiation levels between the wild-type and *infC*Δ55 strains is smaller to begin with). Expression of the CTD did not lead to any improvement in the fidelity function (Fig. 5B and C, compare bars 3 and 5). Therefore, it is evident that the NTD modulates i-tRNA selection and discrimination not only at the level of codon-anticodon interaction but also at the level of recognition of the conserved 3GC base pairs in the i-tRNA anticodon stem. As a control, we also studied initiation by $i\text{-}tRNA_{CUA}$ (Fig. 5A) and noted that the presence of the NTD led to a general increase in acceptance of i-tRNA in the P site of the ribosome (Fig. 5A, bar 4), unlike CTD expression, where the initiation levels were the lowest (Fig. 5A, bar 5).

***In vivo* ribosome antiassociation activity of IF3 domains.** Since the primary function of IF3 is ribosome antiassociation, we wanted to see the *in vivo* effects of expression of the NTD or CTD on the polysome profiles (Fig. S5). Strikingly, the 70S/30S ratios in the *infC*Δ55 strain and the wild-type strain were the same, suggesting that the ribosome antiassociation in the *infC*Δ55 strain was unperturbed. Expectedly, in the background of the *infC*Δ55 strain and in the wild-type background, overexpression of IF3 lowered the 70S/30S ratio. Also, expression of the CTD in the strain *infC*Δ55 background altered the 70S/30S ratio to almost the same extent as overexpression of IF3. Expression of the NTD, however, did not have any significant effect. Therefore, even *in vivo*, the presence of the CTD alone affects antiassociation.

***In vivo* ribosome binding affinity of the IF3 domains.** Although *in vitro* data suggest negligible binding affinity of the NTD to 30S ribosomes (7), in the *infC*Δ55 strain, it improves the fidelity of both the i-tRNA anticodon interaction with the initiation codon and the selection of the i-tRNA via recognition of the 3GC base pairs in its anticodon stem. Hence, we investigated distributions of IF3, NTD, and CTD in the free, 30S, 50S, and 70S fractions of the sucrose density gradient profile of ribosomal preparations by immunoblotting (Fig. 6). In the wild-type strain, most of the IF3 bound to 30S ribosomes and a miniscule fraction was found in the 50S fraction (Fig. 6, panel i). Similarly, in the *infC*Δ55 strain, most of the host-encoded IF3 (deleted for 55 aa from the N terminus) bound to 30S ribosomes (Fig. 6, panel ii). In this strain, expression of CTD revealed that its binding to the 30S ribosomes was at least 2-fold lower than that

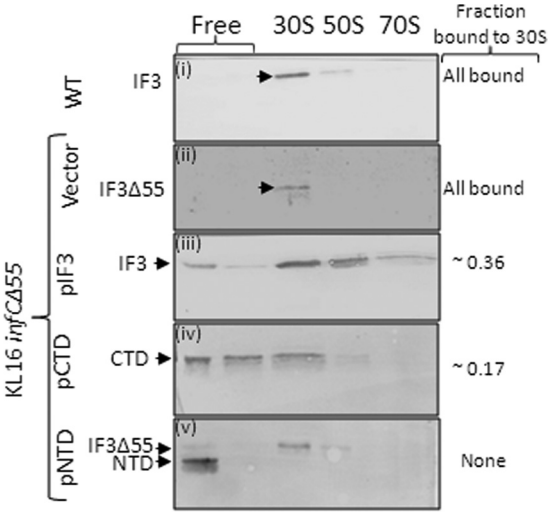

FIG 6 Western analysis of the fractions collected after polysome profiling performed with anti-EcoIF3 antibodies. The pixel values of the relevant bands were quantitated using Multi Gauge V2.3. The proportions of IF3 and its derivatives bound to the 30S subunit (as against the total IF3 seen in the blot) are shown on the right. The vector was pACDH.

of IF3 (Fig. 6, compare panels iii and iv). The immunoblots do not reveal any detectable binding of the NTD to the 30S subunit (Fig. 6, panel v); only the host-encoded IF3 (deleted for 55 aa from the N terminus) is found in the 30S fraction. Therefore, our observations agree with the earlier *in vitro* data (7, 27) and indicate that *in vivo* binding of the NTD to the ribosome must be poor or transient.

DISCUSSION

The *in vivo* analyses presented in this study clearly showed that the CTD but not the NTD of IF3 is essential for cellular viability. However, as seen by the sickness of the *infC*Δ55 strain, the removal of even part of the NTD comes at a severe fitness cost (see Fig. S4 in the supplemental material). Polysome profile analyses (Fig. S5) showed that the CTD is almost as capable of carrying out ribosome antiassociation as the full-length IF3, although it appears to bind to 30S with lower efficiency (Fig. 6). The NTD does not significantly affect ribosome antiassociation (Fig. S5). As expected from *in vitro* observations (7, 27), we did not detect binding of the NTD to the 30S subunit (Fig. 6). Therefore, we can reiterate that the CTD is the domain which establishes contact with the 30S ribosome and modulates ribosome antiassociation whereas the NTD does not play a significant role in these functions. The NTD appears to be responsible for the fidelity function of the intact molecule, despite its inability to establish strong contact with the 30S ribosome.

Petrelli et al. showed that all the functions of IF3 could be performed by its CTD alone provided the concentration of the individual CTD was high enough to compensate for its relatively lower affinity to the ribosome (7). Their conclusions, which were gleaned from *in vitro* experiments, were also supported by nuclear magnetic resonance (NMR) spectroscopy (27, 28), which in turn showed that most of the IF3 residues interacting with the ribosome were present in the CTD. Every IF3 mutation which led to ribosome-binding defects was mapped to the CTD, while *in vivo* studies performed with point mutants of IF3 have consistently indicated the role of residues of the NTD in the fidelity function of IF3 (5, 11, 12, 29, 30). Further, recent cryo-electron microscopy (cryoEM) studies have placed the NTD of IF3 at the elbow region of i-tRNA while the CTD engages in interactions with the 30S subunit and has a steric clash with H69 during formation of the B2a bridge in the 70S ribosome (8). Results of a recent cryoEM study (10) indicated that after mRNA binding, the CTD binds at the P site and occludes the binding site of H69 (Fig. 7A). Subsequent to i-tRNA binding, the NTD moves to the

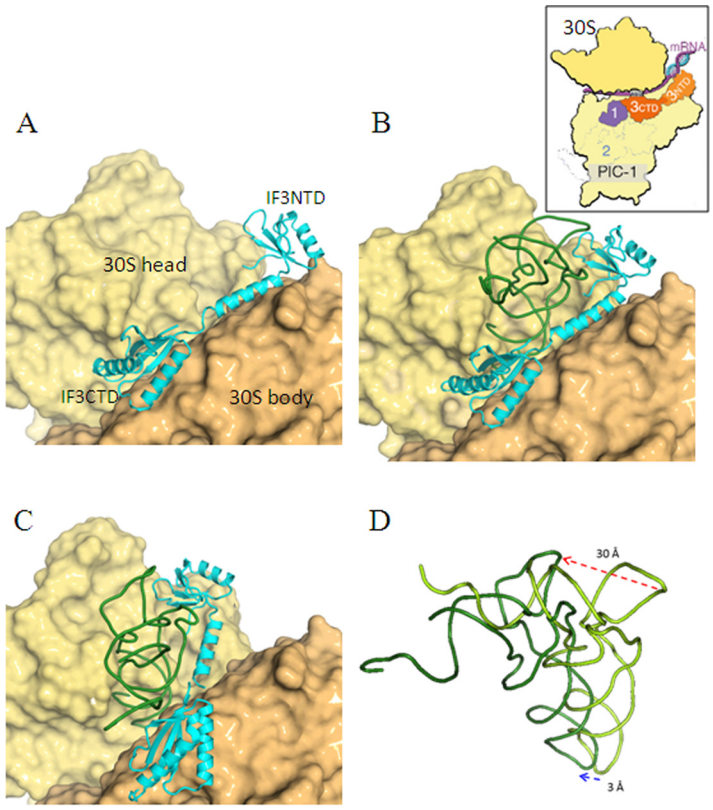

FIG 7 (A) Initial position of IF3 prior to the binding of i-tRNA. The NTD lies on the 30S platform, while the CTD binds at the P site. The 30S head and body are shown in a surface representation in yellow and brown, respectively. (B) Initial position of binding of i-tRNA on 30S and change in position of the NTD of IF3. The NTD moves away from the platform to bind to the elbow of the tRNA. The anticodon stem-loop (ASL) of the tRNA binds in a widened P site, while the elbow is positioned closer to the E site. (C) Final positions of the i-tRNA and IF3 on 30S. The ASL of the tRNA is now accommodated in a narrowed P site, and the position of the elbow is closer to the P site than that shown in panel B. The NTD repositions as it moves with the elbow of the tRNA, and CTD is now positioned away from P site because of the accommodation of the tRNA in the P site. (D) Depiction of the movement of the elbow and anticodon loop regions of the i-tRNA. The initial position, determined as described for panel C, is shown in a light color, and the final position, determined as described for this panel, is shown in a darker shade. The movements are shown by the use of dashed arrows in different colors. The inset shows the positions of IF3 and mRNA on the 30S ribosome. The Protein Data Bank accession numbers for panels A, B, and C are 5LMN, 5LMQ, and 5LMU (10), respectively.

elbow region of the i-tRNA from the platform while the CTD remains at the widened P site without contacting the i-tRNA anticodon stem-loop (Fig. 7B). Following the partial accommodation of i-tRNA in the P site, the CTD positions itself slightly away from the i-tRNA at the P site. At this point, IF3 is wrapped around the i-tRNA and the domains are closest to each other. Consequently, a negatively charged β sheet of the CTD is repelled by the D arm of the i-tRNA in the narrowed P site, while the NTD follows the rotation of i-tRNA and remains bound to the elbow (Fig. 7C). After complete accommodation of the i-tRNA, the CTD and NTD are positioned furthest from each other. The NTD remains bound to the elbow of the i-tRNA, and it may play a role in dislodging the CTD from the P site during the rotation of the i-tRNA. We propose that the binding of the NTD at the elbow of the i-tRNA may allow IF3 to sense a misaccommodated tRNA. A noncognate codon-anticodon interaction or the absence of intact 3GC base pairs at the anticodon stem would render the tRNA unstable due to its dislocation mediated by the NTD, and this would consequently prevent the NTD-driven displacement of the CTD from the H69 binding site, thus preventing 50S binding. This hypothesis is in agreement with the ΔH69 data as well (14). Thus, the positions of the two domains, combined with earlier *in vivo* data (5, 11, 12, 29, 30), seem to indicate that the C-terminal domain

establishes strong contact with the 30S subunits and modulates intersubunit bridge formation and that the N-terminal domain interacts directly with the i-tRNA.

The fidelity function of IF3 is obviously optimal when both domains are present and attached by the linker so that the detection of an accurate i-tRNA at the P site might allow eventual 50S subunit association. However, the NTD is clearly not essential in displacing the CTD from the H69 binding site, as *E. coli* can be sustained on the CTD alone. Further, we have shown that the NTD (100 aa) can improve the fidelity function of IF3Δ55 (125 aa), despite the domains acting in *trans*. Thus, the isolated NTD may interact with the elbow of the i-tRNA even in the absence of a connection with the CTD to regulate the fidelity of initiation. And, on the basis of our observations, we propose that, during the transient binding of the NTD (not detectable by the *in vitro* experiments [Fig. 6] [7]) in the early stages, the linker region of the NTD construct used in our studies may, at least occasionally, displace the linker region of the IF3Δ55 produced in the *infC*Δ55 strain. In the subsequent stages, when the linker region would be found in a position away from the platform (Fig. 7C), there would be no steric conflict with the linker helix of the host-encoded CTD (10).

Thus, our *in vivo* studies suggest that each of the two domains of IF3 has its own unique functions in the cell: the CTD establishes contact with the 30S ribosome and prevents premature formation of the B2a bridge of the 70S ribosome, while the NTD modulates fidelity. Since only the CTD can sustain the cell, we conclude that the ribosome binding and antiassociation functions of IF3 are essential for survival and that the fidelity function of the NTD adds to the fitness of the cell.

MATERIALS AND METHODS

Strains, plasmids, and DNA oligomers. Strains and plasmids used in this study have been listed in Table 1. The DNA oligomers used are listed in Table S2 in the supplemental material. *E. coli* KL16 and its derivatives were grown in 2× yeast extract-tryptone (YT) medium and on 2× YT agar plates (Difco). Unless mentioned otherwise, media were supplemented with ampicillin (Amp; 100 μg/ml), chloramphenicol (Cm; 30 μg/ml), kanamycin (Kan; 25 μg/ml), or tetracycline (Tet; 7.5 μg/ml) as required. Isopropyl-β-D-1-thiogalactopyranoside (IPTG) was used only where mentioned.

Generation of *infC* deletion strains. The Kan^r cassette was amplified from pKD4 using the reverse primers (as required) and the IF3 knockout (ko) fp (forward primer) (Table S2) having regions of homology to the sequences flanking the Kan^r cassette in the template plasmid and the sequences flanking the *infC* gene. IF3 ko rp (reverse primer) 2 was used to generate strain KL16 Δ*infC*, IF3 ko rp was used to generate strain KL16 *infC*Δ55, IF3 ko rp 5 was used to generate strain KL16 *infC*Δ*75*, IF3 ko rp 4 was used to generate strain KL16 *infC*Δ89, and IF3 ko rp 3 was used to generate strain KL16 Δ*infC fs*. PCR amplification reactions were carried out using 10 pmol of each primer and 250 μM deoxynucleoside triphosphates (dNTPs). The reaction mixtures were incubated at 94°C for 4 min followed by 30 cycles of 94°C for 1 min, 45°C for 30 s, and 70°C for 4 min followed by a final extension of 70°C for 10 min. The PCR products were digested with DpnI to remove the template plasmid. An *E. coli* KL16 strain bearing pKD46 (18) was induced with 1 mM arabinose to express recombinases and subsequently transformed by electroporation with 300 ng of linear DNA in cuvettes (0.1 cm gap width) using a Bio-Rad Gene Pulser set at 1.75 kV and 25 μF with a pulse controller set at 200 Ω. YT medium (2×; 1 ml) was added after electroporation. Cells were incubated at 37°C for 4 h with shaking and spread on appropriate selective agar media. The replacement of the *infC* locus by the Kan^r gene was confirmed by colony PCR. Primers *infC* flank fp and *infC* flank rp were used to amplify the genomic DNA of the wild-type strain and the putative knockout strains of *E. coli* by the colony PCR method. The amplification reactions were carried out using 10 pmol of each primer and a 250 μM concentration of each of the dNTPs by heating the samples at 94°C for 5 min followed by 30 cycles of 94°C for 1 min, 53°C for 30 s, and 72°C for 2 min 20 s followed by a final extension of 72°C for 10 min.

Preparation of cell extracts (for SDS-PAGE and immunoblotting). Cells were harvested by centrifugation (Kubota RA2724) at 13,000 rpm for 1 min. The cell pellets were resuspended in 400 μl of TME buffer (25 mM Tris-HCl [pH 8], 2 mM β-mercaptoethanol, 1 mM Na_2EDTA) and subjected to sonication. The conditions of sonication were as follows: amplitude, 40%; pulse, 2 s (on and off 3 times for 25 s each time, with a 1-min gap at each interval). Cells were harvested at 14,000 rpm for 20 min. Supernatant and pellet were obtained. The pellet was resuspended in 200 μl of TME buffer. The sonicator was manufactured by Sonics and Materials Inc., Danbury, CT.

Immunoblot analysis. The requisite amounts of protein were loaded on a 12% or 15% SDS-PAGE gel and transferred onto polyvinylidene difluoride (PVDF) membrane at 15 V for 1 h using a Bio-Rad semidry transfer apparatus. The membrane was soaked in blocking solution (5% skimmed milk–TBST buffer [20 mM Tris-HCl, 0.9% NaCl, 0.1% Tween 20]), kept at room temperature for 1 h, and washed thrice with TBST buffer for 10 min each. Primary antibody was added, and the blot was incubated overnight under rocking conditions at 4°C followed by three washes of 10 min each with TBST buffer. The blot was treated with anti-rabbit goat IgG-alkaline phosphatase (ALP) conjugate (Genei) secondary antibody (1:3,000) for 1 h

under rocking conditions, washed thrice with TBST buffer, and equilibrated with 50 ml 0.1 M Tris-HCl buffer (pH 9) for 10 min. The blot was developed in darkness using a mixture containing 20 ml 0.1 M Tris-HCl buffer (pH 9), 200 μl of 5 mg/ml 5-bromo-4-chloro-3-indolyl phosphate (prepared in 100% dimethyl formamide [DMF]), 200 μl of 30 mg/ml nitroblue tetrazolium (prepared in 70% DMF), and 80 μl 2 M $MgCl_2$. For detection of EcoIF3, rabbit polyclonal anti-EcoIF3 antiserum (1:5,000) was used.

Preparation of cell extracts for CAT assay. The mid-log-phase-grown *E. coli* strains were used for extract preparation as described previously (21). Briefly, four replicates of each strain were grown in 1.5 ml 2× YT broth with required antibiotics at 37°C to the log phase (optical density at 600 nm [OD_{600}], ~0.6 to ~0.7). The cells were harvested and resuspended in 100 μl TME buffer and treated with lysozyme (10 μl of 1 mg/ml solution prepared in TME buffer) and left at room temperature for 10 min. After that, 5 μl of DNase I (a 1 mg/ml solution in 0.1 M $MgCl_2$) was added and the reaction mixture was incubated for 5 min. The contents were flash-frozen in liquid nitrogen and thawed at room temperature. This procedure was repeated twice. The cell debris were then removed by spinning the tubes at 15,400 × *g* for 10 min, 100 μl of supernatant was transferred to a fresh tube containing an equal volume of 2× storage buffer (20 mM Tris-HCl [pH 8.0], 10 mM β-mercaptoethanol, 200 mM NaCl, 80% [vol/vol] glycerol), and the tube was stored at −20°C. The protein content of each extract was quantified by Bradford's assay (31).

Chloramphenicol acetyltransferase assays. *E. coli* cells were grown in 1.5 ml 2× YT broth containing Amp and Tet to the mid-log phase and processed to prepare cell extracts by gentle lysis as described above. A 30-μl reaction mixture comprising 500 mM Tris-HCl (pH 8.0), 5 nmol chloramphenicol, 0.025 μCi (430 pmol) [^{14}C]Cm (PerkinElmer) (specific activity, 57.8 mCi $mmol^{-1}$), and 432 μM acetyl coenzyme A (acetyl-CoA) was incubated for 20 min at 37°C. The reaction was stopped by addition of 300 μl ethyl acetate and thorough vortex mixing. The ethyl acetate phase of the samples was dried and spotted on a silica gel 60 plate (Merck). Thin-layer chromatography (TLC) was performed using a mobile phase consisting of a 95:5 mixture of chloroform and methanol. The TLC plate was scanned using a BioImage Analyzer (FLA5000; Fuji). The pixel values were quantitated in the spots corresponding to 1-acetyl- and 3-acetyl-chloramphenicol (Ac-Cm) and the products (P) of the assay as well as the leftover substrate (S), chloramphenicol (Cm), using Multi Gauge V2.3 software. The CAT activities were calculated as picomoles of Cm converted to Ac-Cm per nanogram of total protein by multiplying the P/(S + P) ratio by the value for the total amount (in picomoles) of Cm taken in the reaction and dividing the product by the value for the total amount of protein in the cell extract. Assays were carried out from four independent colonies, and the mean values were plotted with standard errors. CAT activities are calculated as mentioned in reference 20 relative to the positive control within the same strain and then normalized again against the CAT activity of wild-type strains, as indicated in the figure legends.

Polysome profiling. *E. coli* strains were grown in 100 ml culture to the log phase. Chloramphenicol (100 μg/ml) was added 5 min before harvesting to stabilize the polyribosomes. Cells were rapidly cooled in a salt-ice mixture and immediately pelleted down at 7,000 × *g* for 5 min. The cell pellet was resuspended in 1 ml of buffer A [20 mM HEPES-KOH (pH 7.5), 6 mM $Mg(OAc)_2$, 150 mM $NH_4(OAc)$, 6 mM β-mercaptoethanol, 0.8 mg/ml lysozyme]. The cells were incubated on ice for 30 min. The samples were flash-frozen in liquid nitrogen, thawed in a cold room, and stored at −80°C overnight. On the following day, the samples were thawed in a cold room and centrifuged at 15,000 × *g* for 15 min to remove cell debris. The supernatant was stored as aliquots at −80°C, after flash-freezing in liquid nitrogen. The amount of RNA was measured by checking the absorbance at 260 nm. A sucrose gradient was made by layering approximately 2.5 ml of 35% and 15% sucrose made in buffer B [20 mM HEPES-KOH (pH 7.5), 6 mM $Mg(OAc)_2$, 150 mM $NH_4(OAc)$, 6 mM β-mercaptoethanol] in the tubes using an SW55 rotor. A continuous gradient was created using a BioComp gradient maker by tilting the tubes to 80.5° and rotating at 20 rpm for 1.01 min. An amount corresponding to an OD_{260} of approximately 15 was layered on top of the sucrose gradient and centrifuged at 45,000 rpm for 2 h. After the run, the gradient was analyzed using a BioComp Gradient Analyzer and fractions were also simultaneously collected.

Immunoblot analysis of the fractions collected after polysome profiling. To each fraction collected after polysome profiling, 1.2 volumes of ethanol were added, and the reaction mixtures were kept at −20°C overnight and centrifuged at 18,000 × *g* for 10 min at 4°C. The supernatant was decanted, and the pellet was dried at room temperature (RT), suspended in 1× SDS loading dye, and kept for 1 h. The samples were heated for 1 min at 90°C and loaded on SDS-PAGE gels, and immunoblotting was carried out as described above.

IF3 model. The structure of *E. coli* IF3 was modeled on the basis of the *Thermus thermophilus* IF3 using SWISS-MODEL (32).

SUPPLEMENTAL MATERIAL

Supplemental material for this article may be found at https://doi.org/10.1128/JB.00051-17.

SUPPLEMENTAL FILE 1, PDF file, 1.6 MB.

ACKNOWLEDGMENTS

We thank our laboratory colleagues for their suggestions on the manuscript. We thank Tanweer Hussain of MRC Laboratory of Molecular Biology, Cambridge, United Kingdom, for generating Fig. 7 for us.

Funding for this study was provided by the Department of Biotechnology (DBT),

Ministry of Science and Technology; the Department of Science and Technology (DST), Ministry of Science and Technology; and a DST J.C. Bose Fellowship (to U.V.). We acknowledge the support of the DBT-IISc partnership program, University Grants Commission, New Delhi for the Centre of Advanced Studies, and the DST-FIST level II infrastructure to carry out this work.

REFERENCES

1. Grunberg-Manago M, Dessen P, Pantaloni D, Godefroy-Colburn T, Wolfe AD, Dondon J. 1975. Light-scattering studies showing the effect of initiation factors on the reversible dissociation of Escherichia coli ribosomes. J Mol Biol 94:461–478. https://doi.org/10.1016/0022-2836(75)90215-6.
2. Olsson CL, Graffe M, Springer M, Hershey JW. 1996. Physiological effects of translation initiation factor IF3 and ribosomal protein L20 limitation in Escherichia coli. Mol Gen Genet 250:705–714. https://doi.org/10.1007/BF02172982.
3. Hershey JW. 1987. Protein synthesis, p 613–647. *In* Neidhardt FC, Ingraham JL, Low KB, Magasanik B, Schaechter M, Umbarger HE (ed), *Escherichia coli* and *Salmonella typhimurium*: cellular and molecular biology. American Society for Microbiology, Washington, DC.
4. La Teana A, Gualerzi CO, Brimacombe R. 1995. From stand-by to decoding site. Adjustment of the mRNA on the 30S ribosomal subunit under the influence of the initiation factors. RNA 1:772–782.
5. Sussman JK, Simons EL, Simons RW. 1996. Escherichia coli translation initiation factor 3 discriminates the initiation codon in vivo. Mol Microbiol 21:347–360. https://doi.org/10.1046/j.1365-2958.1996.6371354.x.
6. Hartz D, McPheeters DS, Gold L. 1989. Selection of the initiator tRNA by Escherichia coli initiation factors. Genes Dev 3:1899–1912. https://doi.org/10.1101/gad.3.12a.1899.
7. Petrelli D, LaTeana A, Garofalo C, Spurio R, Pon CL, Gualerzi CO. 2001. Translation initiation factor IF3: two domains, five functions, one mechanism? EMBO J 20:4560–4569. https://doi.org/10.1093/emboj/20.16.4560.
8. Julián P, Milon P, Agirrezabala X, Lasso G, Gil D, Rodnina MV, Valle M. 2011. The Cryo-EM structure of a complete 30S translation initiation complex from Escherichia coli. PLoS Biol 9:e1001095. https://doi.org/10.1371/journal.pbio.1001095.
9. Dallas A, Noller HF. 2001. Interaction of translation initiation factor 3 with the 30S ribosomal subunit. Mol Cell 8:855–864. https://doi.org/10.1016/S1097-2765(01)00356-2.
10. Hussain T, Llacer JL, Wimberly BT, Kieft JS, Ramakrishnan V. 2016. Large-scale movements of IF3 and tRNA during bacterial translation initiation. Cell 167:133–144 e13. https://doi.org/10.1016/j.cell.2016.08.074.
11. Maar D, Liveris D, Sussman JK, Ringquist S, Moll I, Heredia N, Kil A, Blasi U, Schwartz I, Simons RW. 2008. A single mutation in the IF3 N-terminal domain perturbs the fidelity of translation initiation at three levels. J Mol Biol 383:937–944. https://doi.org/10.1016/j.jmb.2008.09.012.
12. Sacerdot C, Chiaruttini C, Engst K, Graffe M, Milet M, Mathy N, Dondon J, Springer M. 1996. The role of the AUU initiation codon in the negative feedback regulation of the gene for translation initiation factor IF3 in Escherichia coli. Mol Microbiol 21:331–346. https://doi.org/10.1046/j.1365-2958.1996.6361359.x.
13. Sacerdot C, de Cock E, Engst K, Graffe M, Dardel F, Springer M. 1999. Mutations that alter initiation codon discrimination by Escherichia coli initiation factor IF3. J Mol Biol 288:803–810. https://doi.org/10.1006/jmbi.1999.2737.
14. Liu Q, Fredrick K. 2015. Roles of helix H69 of 23S rRNA in translation initiation. Proc Natl Acad Sci U S A 112:11559–11564. https://doi.org/10.1073/pnas.1507703112.
15. Shetty S, Shah RA, Chembazhi UV, Sah S, Varshney U. 26 September 2016. Two highly conserved features of bacterial initiator tRNAs license them to pass through distinct checkpoints in translation initiation. Nucleic Acids Res 45:2040–2050. https://doi.org/10.1093/nar/gkw854.
16. Low B. 1968. Formation of merodiploids in matings with a class of Rec-recipient strains of Escherichia coli K12. Proc Natl Acad Sci U S A 60:160–167. https://doi.org/10.1073/pnas.60.1.160.
17. Mangroo D, RajBhandary UL. 1995. Mutants of Escherichia coli initiator tRNA defective in initiation. Effects of overproduction of methionyl-tRNA transformylase and the initiation factors IF2 and IF3. J Biol Chem 270:12203–12209.
18. Datsenko KA, Wanner BL. 2000. One-step inactivation of chromosomal genes in Escherichia coli K-12 using PCR products. Proc Natl Acad Sci U S A 97:6640–6645. https://doi.org/10.1073/pnas.120163297.
19. Varshney U, RajBhandary UL. 1990. Initiation of protein synthesis from a termination codon. Proc Natl Acad Sci U S A 87:1586–1590. https://doi.org/10.1073/pnas.87.4.1586.
20. Arora S, Bhamidimarri SP, Bhattacharyya M, Govindan A, Weber MH, Vishveshwara S, Varshney U. 2013. Distinctive contributions of the ribosomal P-site elements m2G966, m5C967 and the C-terminal tail of the S9 protein in the fidelity of initiation of translation in Escherichia coli. Nucleic Acids Res 41:4963–4975. https://doi.org/10.1093/nar/gkt175.
21. Das G, Thotala DK, Kapoor S, Karunanithi S, Thakur SS, Singh NS, Varshney U. 2008. Role of 16S ribosomal RNA methylations in translation initiation in Escherichia coli. EMBO J 27:840–851. https://doi.org/10.1038/emboj.2008.20.
22. Mandal N, Mangroo D, Dalluge JJ, McCloskey JA, Rajbhandary UL. 1996. Role of the three consecutive G:C base pairs conserved in the anticodon stem of initiator tRNAs in initiation of protein synthesis in Escherichia coli. RNA 2:473–482.
23. Samhita L, Shetty S, Varshney U. 2012. Unconventional initiator tRNAs sustain Escherichia coli. Proc Natl Acad Sci U S A 109:13058–13063. https://doi.org/10.1073/pnas.1207868109.
24. Lesage P, Truong HN, Graffe M, Dondon J, Springer M. 1990. Translated translational operator in Escherichia coli. Auto-regulation in the infC-rpmI-rplT operon. J Mol Biol 213:465–475.
25. Hartz D, Binkley J, Hollingsworth T, Gold L. 1990. Domains of initiator tRNA and initiation codon crucial for initiator tRNA selection by Escherichia coli IF3. Genes Dev 4:1790–1800. https://doi.org/10.1101/gad.4.10.1790.
26. Varshney U, Lee CP, Seong BL, RajBhandary UL. 1991. Mutants of initiator tRNA that function both as initiators and elongators. J Biol Chem 266:18018–18024.
27. Garcia C, Fortier PL, Blanquet S, Lallemand JY, Dardel F. 1995. Solution structure of the ribosome-binding domain of E. coli translation initiation factor IF3. Homology with the U1A protein of the eukaryotic spliceosome. J Mol Biol 254:247–259.
28. Sette M, Spurio R, van Tilborg P, Gualerzi CO, Boelens R. 1999. Identification of the ribosome binding sites of translation initiation factor IF3 by multidimensional heteronuclear NMR spectroscopy. RNA 5:82–92. https://doi.org/10.1017/S1355838299981487.
29. Bruhns J, Gualerzi C. 1980. Structure–function relationship in Escherichia coli initiation factors: role of tyrosine residues in ribosomal binding and functional activity of IF-3. Biochemistry 19:1670–1676. https://doi.org/10.1021/bi00549a023.
30. De Bellis D, Liveris D, Goss D, Ringquist S, Schwartz I. 1992. Structure-function analysis of Escherichia coli translation initiation factor IF3: tyrosine 107 and lysine 110 are required for ribosome binding. Biochemistry 31:11984–11990. https://doi.org/10.1021/bi00163a005.
31. Bradford MM. 1976. A rapid and sensitive method for the quantitation of microgram quantities of protein utilizing the principle of protein-dye binding. Anal Biochem 72:248–254. https://doi.org/10.1016/0003-2697(76)90527-3.
32. Guex N, Peitsch MC, Schwede T. 2009. Automated comparative protein structure modeling with SWISS-MODEL and Swiss-PdbViewer: a historical perspective. Electrophoresis 30(Suppl 1):S162–S173. https://doi.org/10.1002/elps.200900140.